SPECTROSCOPY

Three-dimensional vectorial imaging of surface phonon polaritons

Xiaoyan Li[1], Georg Haberfehlner[2], Ulrich Hohenester[3], Odile Stéphan[1], Gerald Kothleitner[2,4]*, Mathieu Kociak[1]*

Surface phonon polaritons (SPhPs) are coupled photon-phonon excitations that emerge at the surfaces of nanostructured materials. Although they strongly influence the optical and thermal behavior of nanomaterials, no technique has been able to reveal the complete three-dimensional (3D) vectorial picture of their electromagnetic density of states. Using a highly monochromated electron beam in a scanning transmission electron microscope, we could visualize varying SPhP signatures from nanoscale MgO cubes as a function of the beam position, energy loss, and tilt angle. The SPhPs' response was described in terms of eigenmodes and used to tomographically reconstruct the phononic surface electromagnetic fields of the object. Such 3D information promises insights in nanoscale physical phenomena and is invaluable to the design and optimization of nanostructures for fascinating new uses.

Surface phonon polaritons (SPhPs) are mixed electromagnetic and optical phonon waves that propagate at the surface of ionic materials (*1*). In macroscopic solids, they have little influence on the thermodynamic properties, which are dominated by volume acoustic phonons, and hardly couple to the electromagnetic far-field. Therefore, they have been long seen as a scientific curiosity. Recently, they attracted much attention because of their counterintuitive physical properties and their promising applications in photonics and nanophotonics from the mid-infrared (IR) (3 to 8 μm, 155 to 413 meV) up to the far-IR (15 to 1000 μm, 1.2 to 83 meV) (*2*). Their contribution to the physical properties in this range naturally increases with the surface-to-volume ratio (*3*). At the same time, the nanostructuration dramatically influences near-field enhancement and coupling to the far-field.

Therefore, SPhPs directly affect the thermodynamic properties of nanostructured materials. For example, they are responsible for highly coherent emission of silicon carbide (SiC) upon heating, in stark contrast with the conventional incoherent black-body radiation (*4*). They also induce enhanced thermal conduction in thin membranes (*3*) or heat transfer between two nanosurfaces (*5*). These remarkable properties may be favorably applied to the design of phononic metamaterials acting as extremely efficient passive coolers (*6*).

Beyond that, SPhPs concentrate electromagnetic energy at deep subwavelength scales in the same way as surface plasmons, but up to the far-IR region and with exceptionally high-quality factors (*7*), resulting in further intriguing nanophotonic applications, such as superresolution lenses (*2*) or enhanced vibrational spectroscopies (*2*, *7*).

All of these applications rely on the nanostructured electromagnetic field in the vicinity of surfaces of metamaterials or nanoparticles. However, designing or even engineering the electromagnetic local density of states (EMLDOS) for specific functionalities requires the unambiguous visualization of such field modulations at the nanometer scale. This became accessible by means of near-field IR techniques (*8*, *9*). Also, after pioneer works in electron energy loss spectroscopy (EELS) (*10*, *11*), lacking spatial resolution, EELS in a scanning transmission electron microscope (STEM) made it possible to measure phonon spectra at the nanometer (*12*, *13*) then atomic scales (*14*). Nevertheless, intrinsic to those techniques, they only allow for two-dimensional (2D) imaging and do not provide directional field information from the start. Recently, in the visible range, tomographic tilting of plasmonic EELS data in combination with sophisticated eigenmode-based reconstruction algorithms have led to a series of publications (*15*–*17*), culminating in the full 3D and vectorial reconstruction of a plasmonic field at all frequencies in the visible regime (*17*, *18*). The possibility to perform such a reconstruction is deeply rooted in the genuine relation between plasmon excitations and their EMLDOS (*19*), which describes the variation of the square modulus of the eigenfields, projected along arbitrary axes, in space and energy.

Given the strong formal analogy between surface plasmons and phonons (*1*), and having shown the theoretical link between EELS and SPhP EMLDOS (*20*), it was speculated whether a 3D reconstruction of SPhPs properties is also feasible (*20*). The high demands for simultaneous nanometer spatial and milli–electron volt spectral resolution and access to the IR regime could recently be met (*21*), and further advancements in EELS tomographic reconstruction algorithms have now paved the way for a full assessment of the 3D phononic EMLDOS. We allied tilted EELS spectral-imaging with a model-constrained approach to give a comprehensive, 3D vectorial view on the EMLDOS of individual nanometer-scale magnesium oxide (MgO) particles.

We describe the experimental set-up in Fig. 1A. A 60-keV electron beam with an initial energy width of ≈350 meV is filtered by a monochromator to obtain a final energy spread around 7 to 10 meV. This monochromator (*12*) efficiently optimizes the current left after monochromation, with a beam current of a few picoamperes in a sample area of ≈1 nm^2. The nano-object presented in Fig. 1 is a MgO cube with edge length of 191 nm deposited on a 20-nm-thin silicon nitride (Si_3N_4) substrate. The back surface of the substrate was covered with a few-nanometers-thin carbon layer to avoid charge-related issues (supplementary materials, materials and methods). By scanning the electron beam, one can collect high-angle annular dark field (HAADF) images

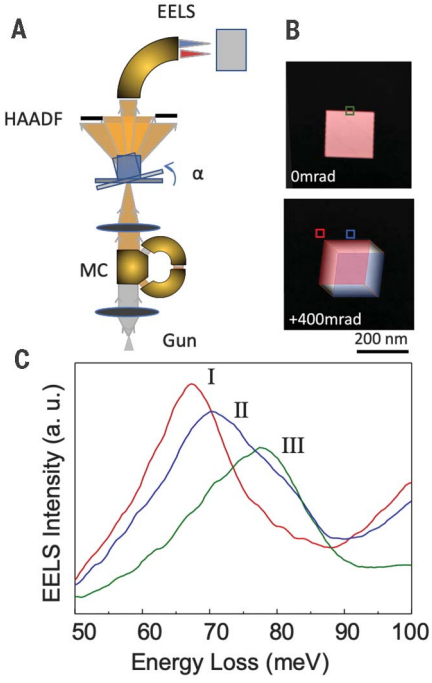

Fig. 1. Tomographic SPhP EELS experiments. (**A**) SPhP tomography set-up. MC, monochromator. (**B**) HAADF images of an MgO cube acquired at two different tilt angles. (**C**) Selected spectra for the two different tilt angles taken at the positions indicated on (B). The ZLP has been removed (materials and methods). Shown is the difference of spectra upon tilt for a fixed beam position (experimental modes II and III). a.u., arbitrary units.

[1]Université Paris-Saclay, CNRS, Laboratoire de Physique des Solides, 91405 Orsay. France. [2]Institute of Electron Microscopy and Nanoanalysis, Graz University of Technology, Steyrergasse 17, 8010 Graz, Austria. [3]Institute of Physics, University of Graz, Universitätsplatz 5, 8010 Graz, Austria. [4]Graz Centre for Electron Microscopy, Steyrergasse 17, 8010 Graz, Austria.
*Corresponding author. Email: gerald.kothleitner@felmi-zfe.at, mathieu.kociak@universite-paris-saclay.fr

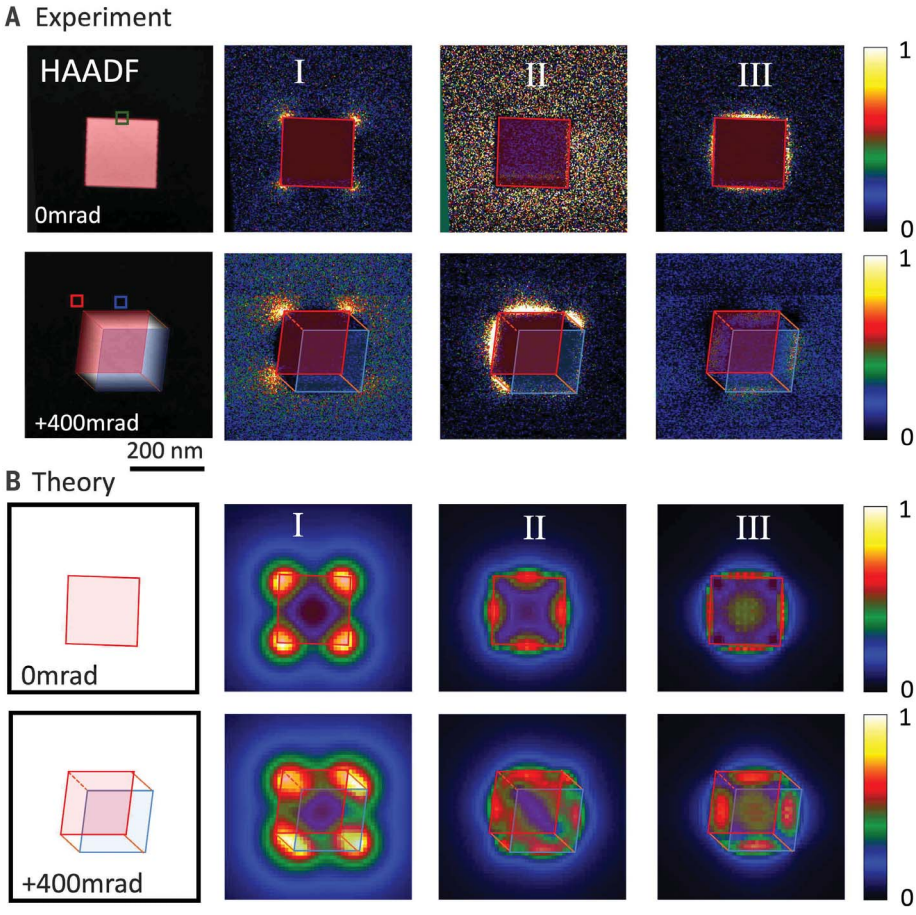

Fig. 2. 2D phonon mapping at different tilt angles. (**A**) (Left) Experimental HAADF images and (right) fitted maps of the main experimental SPhP modes (I, II, and III) for two tilt configurations (0 and 400 mrad) (materials and methods). The face in contact with the substrate is highlighted with a blue square. (**B**) Same for simulations of a cube in vacuum.

that reveal the morphology of the cube. Sample tilting by an angle α allows imaging of the cube under different orientations (Fig. 1B). At each position of the scan, an EELS spectrum was recorded. A complete EELS spectrum (fig. S1) is composed of the zero-loss peak (ZLP), with a strong tail removed (Fig. 1C), and a weak Si_3N_4 phonon around 110 meV, whose left tail can be seen in Fig. 1C. In the reststrahlen band of MgO (upper far-IR), clear spectral responses are extracted at two different tilt angles for two different positions of the electron beam (Fig. 1C). Because the spectral features do change with both the electron beam position and the tilt angle, the selected spectral, spatial, and tilt resolutions of the used setup (materials and methods) has proven adequate to directly resolve signals that are characteristic of the main modes of the cubes (*13*, *20*, *21*). To understand the physical origin of the main spectral features at 68 (experimental mode I), 69 (II), and 78 meV (III), we systematically recorded EELS spectral images (SIs) at different tilt angles. For a first analysis, we present in Fig. 2A intensity maps for the experimental modes I, II, and III for two different tilt angles (full tilt maps are provided in fig. S3). These maps were generated by using a fitting routine for each experimental mode of a SI that has been deconvoluted from the ZLP beforehand (materials and methods) and writing the resulting intensity in the fitted image pixel.

When the electron beam is propagating perpendicular to the faces that are parallel to the substrate (0-mrad tilt), experimental mode I is localized on the four corners. Tilted spectral imaging directly shows a difference in intensity between the signal on corners in vacuum and those on the substrate. The latter is much weaker than the former. The experimental mode II is not directly seen on the 0-mrad map. It is essentially related to the inability of the fitting procedure to resolve experimental mode II because it appears as a weak shoulder on the experimental mode III main peak at zero tilt (*13*). It becomes visible upon tilting (supplementary materials). The signal originates from the edges and again is much weaker for the edges attached to the substrate. Last, the experimental mode III is present at all angles. However, its spatial distribution is more difficult to understand.

As presented in Fig. 2B and in the supplementary materials, we performed simulations for a cube of equal size in vacuum with the boundary element method (*22*) using the MNPBEM package (*23*). The simulations reveal similar features as those in the experimental data and confirm the existence of three different experimental modes (*13*, *20*). The main deviations are the absence of signal inside the cube in the experimental data, owing to the electrons getting scattered out of the spectrometer for large thicknesses, and the obvious absence of asymmetry in the theoretical data because the substrate influence has not been accounted for in the simulations.

To understand the full SPhP response of the cube, we built a tomographic reconstruction method for the EMLDOS inspired by those recently developed in plasmonics (materials and methods and supplementary text) (*17*, *18*). In our approach, we used the quasistatic limit (*24*), which applies because the typical free-space wavelengths of the SPhPs (several tens of micrometers) are much larger than the cube size (fig. S8). The vibrational response of the cube can be described in terms of geometric eigenmodes with spatial distributions $u_k(\mathbf{s})$ of the associated eigencharges, where k labels the eigenmodes and $\mathbf{s}$ is the surface coordinate (*20*, *22*, *24*). Using these

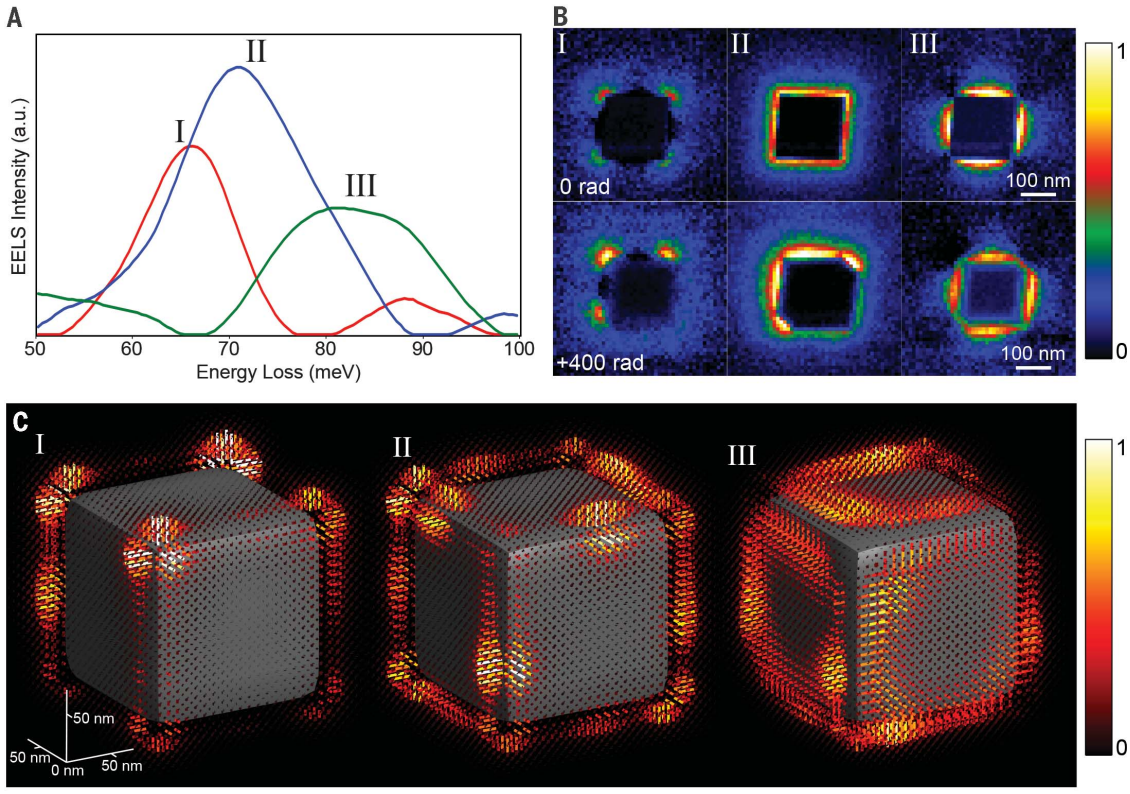

Fig. 3. 3D, fully vectorial reconstruction of the phononic electromagnetic local density of state. (**A**) NMF components extracted from the experimental data. (**B**) Reconstructed NMF maps for the three components at the two angles shown in Fig. 2. (**C**) 3D reconstruction of the EMLDOS seen from the top (the substrate, not shown, is at the bottom of the cube). The polarization of the EMLDOS along three orthogonal directions is shown as needles, in which color and length indicate its intensity.

eigenmodes, the EELS probability can be cast to the form

$$\mathcal{P}_{\mathrm{EELS}} = \sum_k C_k \left| \oint_{\partial\Omega} V_{\mathrm{el}}(\mathbf{s}) u_k(\mathbf{s}) dS \right|^2 \quad (1)$$

where C_k is a mode-dependent coefficient, $V_{\mathrm{el}}(\mathbf{s})$ is the potential associated with the swift electron, and $\partial\Omega$ is the nanocube boundary. The aim of our tomography scheme is to find for each mode I, II, and III the best coefficients C_k and functions $u_k(\mathbf{s})$ for which the reprojected EELS maps of Eq. 1 resemble as closely as possible the experimental ones. Once C_k and $u_k(\mathbf{s})$ are known, we can compute any linear property of the photonic environment, such as the EMLDOS (*20*, *22*, *25*). We express $u_k(\mathbf{s})$ in terms of a simulated reference basis $u_k^0(\mathbf{s})$

$$u_k(\mathbf{s}) \approx \sum_{k'=1}^{n} \mathbb{Q}_{kk'} u_{k'}^0(\mathbf{s}) \quad (2)$$

where $\mathbb{Q}$ is an orthogonal matrix and n is a cutoff for the reference basis states, which is needed for the sake of convergence speed. The basis $u_k^0(\mathbf{s})$ is in principle arbitrary but should be chosen so that the gross features of the modes, such as enhanced charge distributions localized at the corners or edges of the cube, are already encoded to some degree. We used the eigenmodes of a cube in vacuum (Fig. 2B and figs. S7 and S8), calculated by using the boundary element method (*20*, *22*), as a reference eigenbasis. Through the change-of-basis matrix $\mathbb{Q}$, our approach naturally allows the eigenmodes $u_k(\mathbf{s})$ to be reconstructed through complex combinations of the reference eigenmodes, as needed to accommodate for the presence of strong asymmetry in the experimental data. The applicability of this procedure was validated on synthetic data based on a cube in vacuum.

To perform the reconstruction, we used 12 spectral images (12 tilt angles), consisting on 400 by 400 spectra (materials and methods). Despite the massive amount of data, the signal-to-noise ratio was insufficient to proceed directly to the reconstruction. Data treatment by using the non-negative matrix factorization (NMF), following the pioneer work on 3D non-vectorial surface plasmon reconstruction (*15*), leads to the modal signatures shown in Fig. 3A. The NMF spectra are consisting of several peaks, with the most prominent ones corresponding to the I, II, and III experimental modes pointed out in Fig. 1. This allows to confidently associate each experimental mode to an NMF component. An extra peak is seen for the NMF component I around 90 meV, as the manifestation of the imperfect factorization of the NMF (*15*). The corresponding maps displayed in Fig. 3B reproduce the spatial variation already observed on the raw data. Incidentally, the experimental mode II was hardly visible with a simple fitting (Fig. 2A) but is now clearly disentangled thanks to the NMF procedure. Two other NMF components (fig. S5) correspond to the right tail of the zero-loss peak and the left tail of the 110-meV phonon of Si_3N_4 that does not participate to the strong modification of the MgO modes owing to the high indices of the substrate. The NMF components are fitted against the EELS expression (Eq. 1) to get the reconstructed eigenmodes (Eq. 2). From those, the SPhP EMLDOS can be retrieved as displayed in Fig. 3C and fig. S9. Each reconstructed component (I, II, and III) is made up of a sum of reconstructed eigenmodes that are too close in energy to be experimentally disentangled (fig. S10) (*20*). To assure data integrity, modeled reprojected 2D EELS maps calculated from the reconstruction were directly compared with the experimental ones and show very good agreement (fig. S11). Also, the reconstructed EMLDOS is robust against variations in the input experimental data and in the number of reference eigenmodes (fig. S10).

Mode I can therefore be easily interpreted as being mainly localized at the corner ["corner mode" (*13*, *20*, *26*)]. The presence of a substrate is expected to induce a split in two bands of modes, one localized close to the substrate (proximal) and one close to the vacuum (distal)

(*13*, *20*, *26*). The two bands are clearly disentangled spatially, although not spectrally. In particular, the proximal band is strongly damped because of the presence of carbon (*26*) on the substrate (the smaller effect of the substrate in absence of carbon is shown in fig. S4). In addition, some intensity can be seen near the center of some edges. This is because reconstruction includes both resonant [corner localized (*20*)] and nonresonant [edge localized (*20*)] contributions from the different reconstructed modes. This points to the NMF not providing a pure orthogonal decomposition of the different modes. Our reconstruction scheme allows observation of this mixing, although the EELS maps and the reprojection do not. This emphasizes the need to reconstruct a physical observable—the full EMLDOS—that contains the whole physical content of a peculiar system, in contrast to the EELS data, which cannot always be directly interpreted (*24*). The mode II is localized at the edges ("edge mode") (*20*) and is particularly hard to identify (*13*) because of the small energy difference with mode I and the small coupling of the electrons to the mode II field in usual, nontilted, geometry. Last, mode III can be related to surface modes.

This first proof-of-principle visualization of the SPhP EMLDOS should motivate the development of more systematic reconstruction of the full SPhP optical response. Such mapping should be extended to other situations in which the 3D and vectorial information of the electromagnetic density is of importance. This includes extension of the methodology to anisotropic materials such as graphene analogs and transition-metal dichalcogenides. This also includes the possibility to study consistently strong coupling physics, which has recently been unravelled for plasmons and phonons in EELS (*27*). Last, highly monochromated EELS has triggered much hope for its potential applications in vibrational mapping for biological systems (*28*). However, it is well known that the 3D information is mandatory for this purpose (*29*). Therefore, the present method should be adapted to cryomicroscopy to, for example, make it possible to combine ultrastructure characterization with protein vibrational marking in three dimensions.

REFERENCES AND NOTES

1. K. Kliewer, R. Fuchs, *Theory of Dynamical Properties of Dielectric Surfaces*, vol. 27 (Wiley, 1974).
2. J. D. Caldwell *et al*., *Nanophotonics* **4**, 44–68 (2015).
3. Y. Wu *et al*., *Sci. Adv.* **6**, eaba5692 (2020).
4. J. J. Greffet *et al*., *Nature* **416**, 61–64 (2002).
5. B. Song *et al*., *Nat. Nanotechnol.* **10**, 253–258 (2015).
6. E. Rephaeli, A. Raman, S. Fan, *Nano Lett.* **13**, 1457–1461 (2013).
7. M. Autore *et al*., *Light Sci. Appl.* **7**, 17172 (2018).
8. R. Hillenbrand, T. Taubner, F. Keilmann, *Nature* **418**, 159–162 (2002).
9. R. Zhang *et al*., *Nature* **498**, 82–86 (2013).
10. H. Raether, *Excitation of Plasmons and Interband Transitions by Electrons*, vol. 88 (Springer, 2006).
11. H. Boersch, J. Geiger, W. Stickel, *Phys. Rev. Lett.* **17**, 379–381 (1966).
12. O. L. Krivanek *et al*., *Nature* **514**, 209–212 (2014).
13. M. J. Lagos, A. Trügler, U. Hohenester, P. E. Batson, *Nature* **543**, 529–532 (2017).
14. F. S. Hage, G. Radtke, D. M. Kepaptsoglou, M. Lazzeri, Q. M. Ramasse, *Science* **367**, 1124–1127 (2020).
15. O. Nicoletti *et al*., *Nature* **502**, 80–84 (2013).
16. S. M. Collins *et al*., *ACS Photonics* **2**, 1628–1635 (2015).
17. A. Hörl *et al*., *Nat. Commun.* **8**, 37 (2017).
18. G. Haberfehlner *et al*., *Nano Lett.* **17**, 6773–6777 (2017).
19. F. J. García de Abajo, M. Kociak, *Phys. Rev. Lett.* **100**, 106804 (2008).
20. H. Lourenço-Martins, M. Kociak, *Phys. Rev. X* **7**, 041059 (2017).
21. M. J. Lagos *et al*., *Microscopy (Oxf.)* **67** (suppl_1), i3–i13 (2018).
22. F. J. García de Abajo, J. Aizpurua, *Phys. Rev. B Condens. Matter* **56**, 15873–15884 (1997).
23. U. Hohenester, *Comput. Phys. Commun.* **185**, 1177–1187 (2014).
24. U. Hohenester, *Nano and Quantum Optics* (Springer, 2020).
25. G. Boudarham, M. Kociak, *Phys. Rev. B Condens. Matter Mater. Phys.* **85**, 245447 (2012).
26. S. Mazzucco *et al*., *Nano Lett.* **12**, 1288–1294 (2012).
27. L. H. G. Tizei *et al*., *Nano Lett.* **20**, 2973–2979 (2020).
28. P. Rez *et al*., *Nat. Commun.* **7**, 1 (2016).
29. W. Kukulski, M. Schorb, M. Kaksonen, J. A. Briggs, *Cell* **150**, 508–520 (2012).

ACKNOWLEDGMENTS

X.L., O.S., and M.K. thank M. Walls and A. Gloter for help in preparing the sample and acknowledge the joint effort of the STEM team in Orsay. M.K. thanks F. De La Peña for insightful discussions on the NMF factorization and the physics of the nanocubes plasmons. **Funding:** This work has received support from the National Agency for Research under the program of future investment TEMPOS-CHROMATEM with the reference no. ANR-10-EQPX-50. This project has received funding from the European Union's Horizon 2020 Research and Innovation Program under grant agreements 823717 (ESTEEM3) and 101017720 (EBEAM) and from the Austrian Science fund FWF under project P 31264. **Author contributions:** G.K. and M.K. conceived the project. G.K, M.K., O.S., and X.L. designed the experiments. X.L. and M.K. performed the experiments. X.L. and G.H. performed the data analysis. U.H. designed the theory, and G.H. and U.H. performed the reconstructions. All authors participated in the results analysis and contributed to the preparation of the manuscript. **Competing interests:** The authors declare no competing interests. **Data and materials availability:** All data necessary for evaluating the conclusions of the paper are included in the main text and/or the supplementary materials.

SUPPLEMENTARY MATERIALS

science.sciencemag.org/content/371/6536/1364/suppl/DC1
Materials and Methods
Supplementary Text
Figs. S1 to S11
References (*30*–*36*)

7 December 2020; accepted 12 February 2021
10.1126/science.abg0330

Three-dimensional vectorial imaging of surface phonon polaritons

Xiaoyan Li, Georg Haberfehlner, Ulrich Hohenester, Odile Stéphan, Gerald Kothleitner and Mathieu Kociak

Science **371** (6536), 1364-1367.
DOI: 10.1126/science.abg0330

Mapping nanostructure surface excitations

Atomic vibrations (phonons) govern many physical properties of materials, especially those related to heat and thermal transport. They also provide fingerprints of the chemistry of a wide variety of materials, from solids to molecules. The behavior of phonons in nanostructures can be appreciably modified because of confinement effects. Li *et al.* combined several electron microscopy techniques to map out the phonon-polariton excitations across the surface of magnesium oxide nanostructures with high spatial, spectral, and angular resolution. The reconstruction of the surface excitation maps in three dimensions will be useful for understanding and optimizing the properties of the nanostructured materials for advanced functionality.

Science, this issue p. 1364